Theoretical and Applied Climatology
https://doi.org/10.1007/s00704-021-03669-y

ORIGINAL PAPER

Long-term climatic water availability trends and variability across the African continent

Charles Onyutha[1]

Received: 8 December 2019 / Accepted: 24 May 2021

Abstract
This study analyzed trends and variability in climatic water availability (CWA) across the African continent using monthly precipitation and potential evapotranspiration (PET) over the period 1901–2015. Climatic water availability was characterized in terms of precipitation minus PET totals. Predictability of the variation in CWA was tested using climate indices. Large positive values of the CWA (or few drought incidents) were confined to areas (such as sub-region along the Gulf of Guinea, the western part of the equatorial region, and the Ethiopian Highlands) that receive large amounts of precipitation. Drought incidence in these areas was generally low and characterized by severity in the range 0–44% indicating moderate to extreme wetness. Areas which experienced increasing CWA or wetting trends were confined within the Tropics. These wetting trends were mostly insignificant ($p > 0.05$). Drying trends (or decreasing CWA) occurred mainly in areas outside the Tropics. These drying trends (especially in the CWA of the months from April to September) were mainly significant ($p < 0.05$) over the Sahara desert. CWA variability in the southern and eastern parts of Africa was negatively and positively correlated with Niño 3, respectively. Variability of the East African CWA was also positively correlated with the Indian Ocean Dipole (IOD). CWA variability in West Africa (or Sahel) was negatively correlated with Niño 3. Variability of West African CWA was also linked to changes in the sea surface temperature over the Atlantic Ocean. Based on multiple linear regression, predictability of variation in CWA using combinations of climate indices varied across regions and among time scales. For instance, using combination of IOD and Niño 3 as predictors, up to about 40% and less than 10% of the total variance in CWA across East Africa and area north of the Sahel belt could be explained, respectively.

1 Introduction

Due to climate variability, wet and dry climatic conditions tend to occur in a clustered way in time (Onyutha and Willems 2017). Across the continent of Africa, disasters related to both surplus and scarcity of water occur. Examples of such rainfall-based disasters include landslides, floods, and droughts. Prolonged dry conditions can be consequential to low rainfall total and persistent high temperature. Temperature regulates potential evapotranspiration (PET) rate as an important factor for determining crop water requirements. Prolonged dry conditions thwart struggles aimed at tackling challenges of food insecurity especially in the sub-Saharan Africa (SSA) where farming is mainly based on rain-fed cropping system. Apart from crop failures, prolonged drought is liable for a number of deaths of livestock. Drought tends to be aggravated by an increase in demand for resources such as water (for crops, livestock, and human consumption) as a result of climate variability as well as anthropogenic factors (Zhao and Dai 2015). Compared with other regions of the world, the SSA is the least prepared region for weather-related risks such as prolonged drought. Despite the dry conditions across Africa, precipitation in areas such as the Ethiopian Highlands and the equatorial region tends to be of larger amounts than those over other parts of the continent. Areas with large annual precipitation totals tend to experience rainfall-based disasters such as floods and landslides. Impacts of climate variability on meteorology (for instance, in terms of changes in the frequency of drought and flooding events) across the various climatic regions of the African continent are disproportionate.

Planning of predictive adaptation to climate variability impacts on practices (such as agriculture) which depend on precipitation seasonality require comprehensive information on the historical changes in climatic water availability (CWA)

✉ Charles Onyutha
conyutha@kyu.ac.ug; conyutha@gmail.com

[1] Department of Civil and Environmental Engineering, Kyambogo University, P.O. Box 1, Kyambogo, Kampala, Uganda

Published online: 29 June 2021

across Africa. In this study, CWA referred to the precipitation minus PET. Water scarcity (or precipitation deficit) results when precipitation is less than PET. On the other hand, surplus of precipitation can be obtained when PET is less than precipitation. Thus, CWA is directly relevant for determination of crop water requirements. Analyzing CWA trends and variability requires long-term precipitation and PET series which should be of high spatial resolution. Most past studies on dry and wet conditions in Africa were mainly based on short-term observed data and confined to regional scale or even small areas. Examples of such studies include Klutse et al. (2021), Gebremeskel et al. (2019), Uhe et al. (2017), Onyutha (2017), Lyon (2014), Nicholson (2014), Mwangi et al. (2014), Viste et al. (2013), Omute et al. (2012), Hillbruner and Moloney (2012), Ntale and Gan (2003), Verschuren et al. (2000), and Shanko and Camberlin (1998). However, there are a few studies (for instance, Sheffield et al. 2014; Shiferaw et al. 2014; Rojas et al. 2011) on drought considering large areas or the entire continent of Africa. Even in such studies, not both trends and climate variability were considered. Furthermore, the past studies on drought across Africa did not generally quantify drought incidence across the continent and neither did they consider the need to assess linkages of the variation of wet and dry conditions to changes in large-scale ocean–atmosphere conditions.

For monitoring of meteorological dry and wet conditions, a number of methods exist including the Standardized Precipitation Index (SPI) (McKee et al. 1993) and Standardized Precipitation Evapotranspiration Index (SPEI) (Vicente-Serrano et al. 2010). The SPI makes use of precipitation. However, the SPEI can be derived based on the difference between precipitation and evapotranspiration. The main problem with these common methods is that they yield skewed indices (Onyutha 2017). To address this issue, some non-Gaussian distributions such as gamma distribution, generalized extreme value distribution, and log-logistic distribution are assumed and transformed to derive indices which can be used to characterize dry and wet conditions. Reduction in the reliability of the derived indices from the common methods such as SPI and SPEI are further compounded not only by the influence of selection of the best non-Gaussian distribution on the indices but also the uncertainty stemming from estimations of the assumed distribution parameters. In light of the problems related to reliability of the indicators of dry and wet conditions, the use of non-parametric drought indices can be explored.

Therefore, the aim of this paper was to analyze spatial and temporal changes in dry and wet conditions across Africa. Furthermore, this paper focussed on (i) mapping out spatial differences of drought indices considering various time scales and (ii) investigating the predictability of the variation in dry and wet conditions across the different regions of the continent.

2 Materials and methods

2.1 Data

2.1.1 Precipitation and PET

Gridded ($0.5° \times 0.5°$) monthly precipitation and PET Climatic Research Unit (CRU) Time-Series (TS) version 4.0 (CRU TS4.0) (Harris et al. 2014) covering the period 1901–2015 were downloaded via the link https://crudata.uea.ac.uk/cru/ (accessed: 18th June, 2017). The CRU TS4.0 data extracted for this study covered the region 21° W–57° E and 40° N–40° S in the east–west and north–south directions, respectively. Datasets at grid points over land were thoroughly checked and confirmed to have no missing values. At each grid point, CWA was obtained and used to derive drought indices using the procedure described next.

2.1.2 Climate indices

Increase/decrease in sea level pressure (SLP) can bring about dry/wet conditions. However, the sea surface temperature (SST) engenders an imbalance in the heat-flux field thereby leading to anomalous atmospheric circulation and rainfall patterns (Horel 1982). A total of four climate indices were selected for an insight on how variation in temperature or pressure from the various oceans influence wet and dry conditions across the African continent. The selected climate indices included the North Atlantic Oscillation (NAO) index (Jones et al. 1997), Atlantic Multidecadal Oscillation (AMO) index (van Oldenborgh et al. 2009), Niño 3 index (Rayner et al. 2003; Trenberth 1997), and the Indian Ocean Dipole (IOD) index. The NAO index is the normalized SLP difference between SW Iceland (Reykjavik), Gibraltar, and Ponta Delgada (Azores). The IOD index refers to the anomalous SST difference between the western (50° E to 70° E and 10° S to 10° N) and the southeastern (90° E to 110° E and 10° S to 0° N) equatorial Indian Ocean. The Niño 3 characterizes the SST across the tropical Pacific region (90°–150° W and 5° N–5° S). The AMO index refers to the SST averaged over 25° N–60° N, 7° W–70° W minus the regression on global mean temperature (van Oldenborgh et al. 2009). The AMO, NAO, and Niño 3 were downloaded on the 13th November 2018 from the website of https://www.esrl.noaa.gov/. However, the IOD index downloaded on the 20th January 2014 via the link http://www.jamstec.go.jp/frcgc/research/d1/iod was used.

It is worth noting that there has been a considerable debate on which forcing mechanism control AMO or the

North Atlantic SST variations (Folland et al. 1986; Delworth and Mann, 2000; Parker et al. 2007; Mann et al. 2009; Otterå et al. 2010; Knudsen et al. 2014). However, AMO was considered in this study solely for testing the predictability of the variation in wet and dry conditions. In other words, determining which forcing mechanism is responsible for pacing the AMO was out of the scope of this study.

2.2 Analysis of drought incidence

Drought incidence can be taken to mean the commonness of drought at a place or over a given period (Onyutha 2020a). Incidence was determined at each grid point. Drought incidence was computed as the ratio of the number of all the months with the CWA below the threshold to the total number of months within the period (under consideration) expressed as percentage (Onyutha 2017). For CWA obtained using daily data, the incidence could be computed using number of days instead of months. However in this study, the thresholds were set to − 1 mm, − 5 mm, − 25 mm, and − 50 mm of the CWA.

2.3 Analysis of trend

The magnitude (m) of the linear variation of the CWA in each month with time was computed using (Theil 1950; Sen 1968)

$$m = \text{Median}\left(\frac{y_j - y_i}{j-i}\right),\ \forall i < j \tag{1}$$

The significance of the trend slope quantified in the CWA of each month was assessed by testing the null hypothesis H_0 (no trend) using the method developed by Onyutha (2021) such that for a given dataset Y of sample size n, we can rescale Y into series d_y in terms of

$$d_{y,i} = n - w_{y,i} - 2t_{y,i} \text{ for } 1 \le i \le n \tag{2}$$

where $t_{y,i}$ denotes the number of times the ith observation exceeds other data points in Y. In the same line, $w_{y,i}$ refers to number of times the ith data point appears within Y. For instance, a given dataset Y with $n = 10$ such that $y = \{4, 5, 2, 3, 5, 1, 8, 7, 6, 4\}$ yields $t_y = \{3, 5, 1, 2, 5, 0, 9, 8, 7, 3\}$, $w_y = \{2, 2, 1, 1, 2, 1, 1, 1, 1, 2\}$, and $d_y = \{2, -2, 7, 5, -2, 9, -9, -7, -5, 2\}$.

The trend statistic T was given by (Onyutha 2021)

$$T = \sum_{j=1}^{n}\sum_{i=1}^{j} e_{y,i} \tag{3}$$

where

$$e_{y,i} = d_{y,i} \times \sqrt{(n-1) \times \left(\sum_{i=1}^{n}\left(d_{y,i}\right)^2\right)^{-1}} \text{ for } 1 \le i \le n \tag{4}$$

The mean of T is zero and for large n, the distribution of T is approximately normal with the variance of T given by (Onyutha 2021)

$$V(T) = \frac{n\left(n^2 - 1\right)}{12} \tag{5}$$

The standardized test statistic Z which follows the standard normal distribution with mean (variance) of zero (one) is given by

$$Z = \frac{T}{\sqrt{\lambda \times V(T)}} \tag{6}$$

where the term λ with its details provided by Onyutha (2021) corrects $V(T)$ from the influence due to persistence in the data. The mean of T is zero and the H_0 (no trend) is rejected for $|Z| > \left|Z_{\alpha/2}\right|$ where $Z_{\alpha/2}$ denotes the standard normal variate at the selected α; otherwise, the H_0 is not rejected at α. In this study, α was taken as 0.05 thereby corresponding with the Z value of 1.96. This method for trend analysis can be found implemented in a MATLAB-based tool called CSD-VAT (Onyutha 2021) which can be downloaded via https://www.researchgate.net/publication/332798309 (accessed: 25th May 2021).

2.4 Standardized non-parametric indices of precipitation and evaporation

2.4.1 Temporal aggregation of the data

This procedure starts with the selection of the relevant time scale H such as 1, 3, 6, and 12 months. Using a particular H, an aggregation of the given monthly series X (or precipitation minus PET, river flow, or soil moisture) of sample size n can be performed in terms of

$$a_k = \frac{1}{b_k}\sum_{i=g}^{f} x_i \text{ for } 1 \le k \le n \text{ and } g \le i \le f \tag{7}$$

where a_k and b_k are respectively the mean and number of the x_i's in the kth time slice. While k is varied from 1 to n, determination of b_k and the computation of a_k follow a stepwise procedure. In the first step, for a selected H, v can be computed using $v = 0.5 \times (H + 1)$ and $v = 0.5 \times H$ when H is odd and even, respectively.

In the second step, values of the terms f, g, and b_k are assigned based on how k is comparable with v such that

$$\left.\begin{array}{l} \text{if } \ k < v, g = 1,\ f = H + k - v - 1,\ b_k = f \\ \text{if } \ v \le k \le (n - v),\ g = k - v + 1,\ f = k + v,\ b_k = H \\ \text{if } \ (n - v) < k \le n,\ g = k - v + 1,\ f = n,\ b_k = n - k + v \end{array}\right\} \tag{8}$$

To apply Eqs. (7)–(8), a step-wise procedure can be adopted. For instance, if $H=12$, it means $v=6$. We can vary i from 1 to n, and let us assume that $n=100$. For each k, the terms g and f of Eq. (7) can be determined using three conditions from Eq. (8). Next, as explained in Onyutha (2019), an illustration of how the terms g and f can be determined for every k (which is varied by setting $k=1, 2, \ldots, 100$) using $H=12$, $v=6$, and $n=100$ is as follows:

i) If $k=1$, it means $k<v$ and therefore, using the first conditional part of Eq. (8), $g=1$, and $f=12+1-6-1=6$. Thus for $k=1$, the summation in Eq. (7) considers x from i=1 (the 1st) to i=6 (the 6th) value.
ii) If $k=15$, it means $k>v$ and thus, using the second conditional component of Eq. (8), $g=15-6+1=10$, and $f=15+6=21$. In other words, for $k=15$, the summation in Eq. (7) considers x from the 10th to the 21st value.
iii) If $k=96$, it means $k>(n-v)$ and $k\leq n$; thus, considering the third conditional part of Eq. (2), $g=96-6+1=91$, and $f=100$. This means that for $j=96$, the summation of x according to Eq. (7) is done from i=91 (the 91st) to i=100 (the 100th) value.

2.4.2 Non-parametric rescaling of the aggregated data

After temporal aggregation of a resulting from Eq. (7), we rescale a into series d with a mean of zero using Eq. (2).

Let standardized non-parametric indices of precipitation and evaporation (SNIPE) be denoted by S. To obtain S with the mean (variance) of zero (one), we can make

$$o_i = \frac{d_i \times |d_i|}{n} \text{ for } 1 \leq i \leq n \tag{9}$$

$$c = \left(\frac{1}{n-1} \sum_{i=1}^{n} o_i^2 \right)^{\frac{1}{2}} for 1 \leq i \leq n \tag{10}$$

such that

$$S_i = \frac{o_i}{c} \text{ for } 1 \leq i \leq n \tag{11}$$

The classification of the dry and wet conditions based on SNIPE computed using 100-year monthly data can be seen in Table 1. The bounds for S depend on n.

2.5 Correlation between SNIPE and climate indices

The co-variation of CWA and large-scale ocean–atmosphere conditions was assessed in terms of correlation analyses. It is worth noting that the relationship between independent and dependent variables may be linear or non-linear. A plausible step would be to first determine which model best describes the relationship between the two variables. This study considered about 13,000 grid points at which CWA was computed. Therefore, linear model was selected for brevity to test the predictability of the variation in dry and wet conditions. Eventually, for a selected time scale, correlation between SNIPE and the series resulting from the application of Eq. (11) to each of the climate indices was assessed.

Table 1 Classification of dry and wet conditions based on SNIPE

Category	From	To	Probability %
Dry conditions			
Exceptionally dry	<-2.2314		≤ 3.30
Extremely dry	-2.0000	-2.2314	3.31
Severely dry	-1.5000	-1.9999	5.40
Moderately dry	-0.5000	-1.4999	12.95
Mildly dry	0.0000	-0.4999	35.21
Wet conditions			
Mildly wet	0.0000	0.4999	35.21
Moderately wet	0.5000	1.4999	12.95
Severely wet	1.5000	1.9999	5.40
Extremely wet	2.0000	2.2314	3.31
Exceptionally wet	>2.2314		≤ 3.30

Given the possibility that wet or dry conditions at a location can be influenced by two or more drivers, multiple linear regression equation (MLRE) was used to explore the predictive relationship between SNIPE and various combinations of rescaled climate indices as predictors. Here, rescaled climate indices refer to the series obtained after applying Eq. (11) to the climate indices. The mismatch between the rescaled climate indices and SNIPE was reduced through the mean squared error minimization using an adjusted coefficient of determination R^2 (Ezekiel 1930) as the statistical "goodness-of-fit" measure. The MLRE used was

$$Y_i = A_0 + A_1 X_{1,i} + A_2 X_{2,i} + A_3 X_{3,i} + A_4 X_{4,i} + \varepsilon \tag{12}$$

where Y_i is the ith value of the dependent variable, A_0 is the intercept term while A_1, A_2, A_3, A_4 are the slope coefficients of the first, second, third, and fourth independent variable, respectively, and ε denotes the error term. The four independent variables were the climate indices including NAO, AMO, IOD, and Niño 3. The index i was varied from 1 to q where q is the sample size of the climate index with the smallest number of data points.

3 Results and discussion

3.1 Long-term mean of the difference between precipitation and PET

Figure 1 shows the spatial distribution of long-term mean of the CWA. It is noticeable that the Sahara desert or region

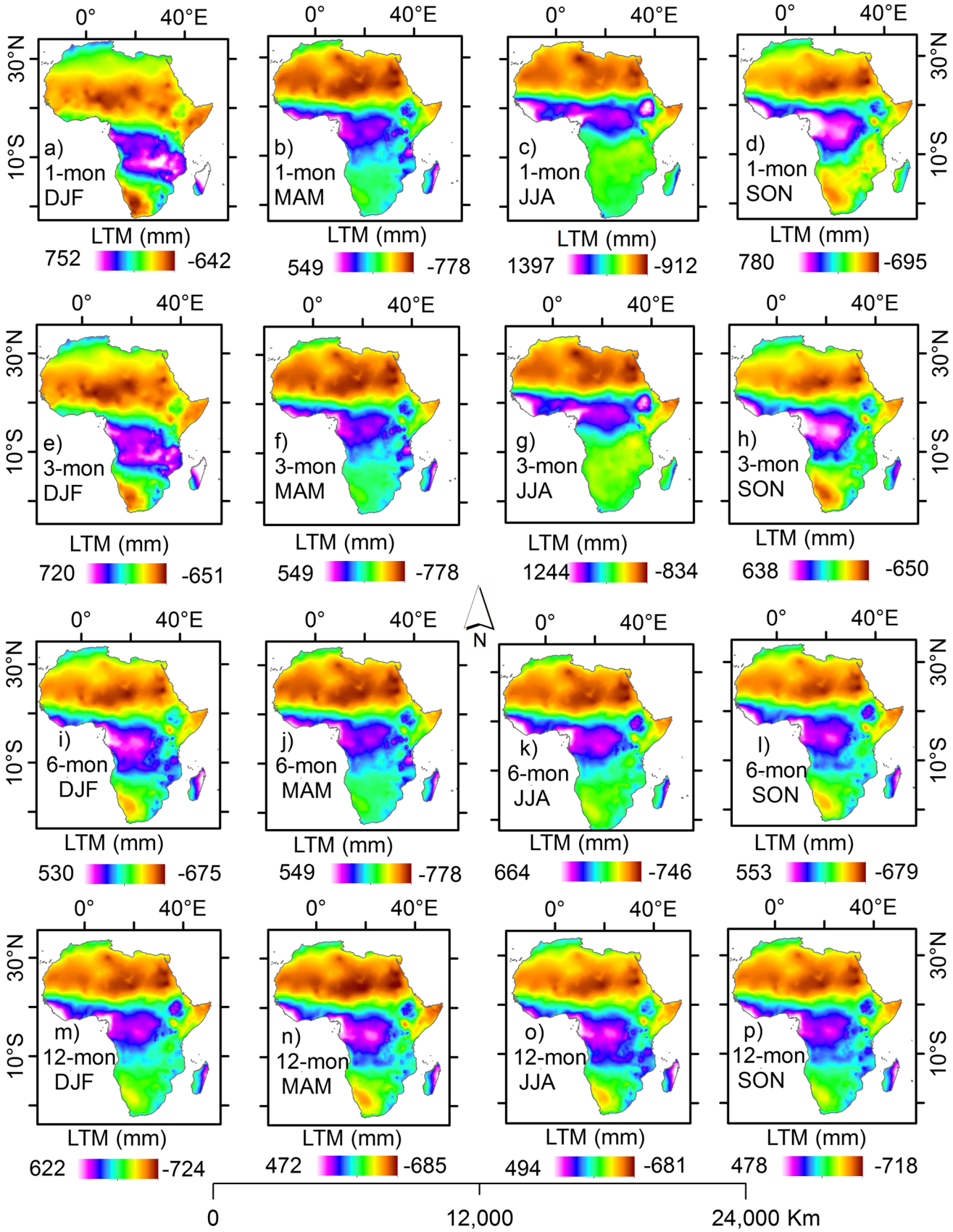

Fig. 1 Long-term mean (LTM) of the CWA in various seasons extracted after aggregation based on a–d 1-month, e–h 3-month, i–l 6-month, and m–p 12-month time scales

North of 10° N was characterized by a large negative CWA (Fig. 1a–p). This region is very dry due to the always low mean annual precipitation (Almazroui et al. 2020). Large positive values of the CWA were confined to areas that receive large amounts of precipitation including the western part of the equatorial region, sub-region along the Gulf of Guinea, and the Ethiopian Highlands (Fig. 1a–p). Results among seasons were more comparable for 12-month than 3-month time scale (Fig. 1a–d, m–p). This can be visually confirmed by noticing the spatial extents of the areas with positive values of the CWA. This means that an increase in time scale beyond the length of the longest season in a year eliminates the possible influence of seasonality on the CWA. Each season considered comprised 3 months. When 4-month time scale was used, the shifts in the region with positive values of CWA can be clearly noticed for the December-January–February (DJF), March–April-May (MAM), June-July–August (JJA), and September–October-November (SON) seasons. This suggests that the results of drought based on a small window (for instance, with the length of 3 months) can be influenced by the effect of seasonal fluctuations in the data.

3.2 Drought incidence

Figure 2 shows drought incidence for selected time scales and thresholds. For simplicity, the severity of drought based on incidence was categorized as 0–9% (extremely wet), 10–19% (severely wet), 20–44% (moderately wet), 45–55% (near normal dry/wet condition), 56–69% (moderately dry), 70–89% (severely dry), and 90–100% (extremely dry). Regardless of the threshold or time scale, areas with extremely dry conditions are confined to the Sahara and Namib deserts as well as the Horn of Africa. It is noticeable that for a given time scale, as the threshold becomes large in magnitude or absolute term (for instance, from − 1 to − 5 mm), the geographical coverage especially for low incidence in the range 0–5% also increases (Fig. 2a–p). However, for a given threshold, as the aggregation level becomes large, the area with low incidence in the range 0–9% also increases. From Fig. 2, it is evident that areas with low drought incidence can be noticed across the Congo basin, the Ethiopian Highlands, as well as the sub-region along the Gulf of Guinea. Prolonged high incidence of drought has wide ranging implications. It could indicate insufficient soil moisture to support small-scale farming something on which subsistence of the local population depends. Furthermore, high drought incidence also indicates lack of pasture to support raring of livestock. These present worrying situations in fighting food insecurity, a challenge which is already at a formidable level especially in the SSA. Perhaps, improved drought-resistant crops could be adopted by the farmers. Importantly, to improve on the household income, the local population could also get involved in non-farm activities that generate income.

Figure 3 shows magnitudes of linear increase or decrease in the CWA across the continent. The largest part of the continent was characterized by decreasing trend in CWA (Fig. 3a–l). Decreasing trend in CWA indicates an increase in climatic dryness. This can be attained under conditions of decreasing precipitation and increasing PET. Large part of Africa was also found to be characterized by decreasing precipitation especially over the period 1961–2015 (Onyutha 2020b). Increasing temperature (a key determining factor) for PET rate was also found in most areas of the African continent over the period 1901–2015 (Onyutha 2020b). In another study, temperature from 1961 to 2000 across Sahel as well as along the Coast of Guinea exhibited increasing trend (Ilori and Ajayi 2020). Areas which experienced increasing trend in CWA were confined within the Tropics (Fig. 3a–l). The largest increases in CWA in January (Fig. 3a) were confined to Gabon, Republic of Congo, and areas around the Lake Victoria. In February and March (Fig. 3b–c), decrease in CWA was over the eastern part of the continent. The April CWA decreased mainly along the Equator (Fig. 3d). From May to September, decreasing trends in CWA were mainly in the region between 5° N and 15° N (Fig. 3e–i). However, the same region also has patches of areas with increasing trends in CWA. Increasing trend in CWA indicates transition from dry to wet conditions. In other words, positive trend in long-term CWA shows shift from climatic condition characterized by water scarcity to water surplus or availability.

Significance of the CWA trends can be seen in Fig. 4. It is noticeable that areas with significant decreasing CWA trends ($p < 0.05$) were confined to the belt along the Tropic of Capricorn from May to August (Fig. 4e–h), the southernmost part of the continent from September to December (Fig. 4i–l). Sahara desert also mainly exhibited significant decrease in CWA of various months espacially from April to October (Fig. 4d–j). Significant increases ($p < 0.05$) in CWA over Gabon were obtained in July and October (Fig. 4g, j).

3.3 SNIPE

Figure 5 shows, at the location with longitude = 25° and latitude = − 24.75°, the variation of SNIPE with time scales. Due to the effect of temporal aggregation of CWA, it is evident (Fig. 5a–c) that an increase in time scale leads to (i) reduction in the SNIPE variability, (ii) increase in drought duration (or period over which the SNIPE is consecutively negative), and (iii) reduction in the frequency (or number) of drought events. Notable drought events at the location under consideration occurred in the 1940s and the early 1980s. However, wet conditions occurred in the 1930s, 1950s, and the 1970s.

The use of different time scales is relevant for careful planning of various water resources managemetn applications which can be affected by scarcity of water. Such applications include crop production, livestock raring, and reservoir operations.

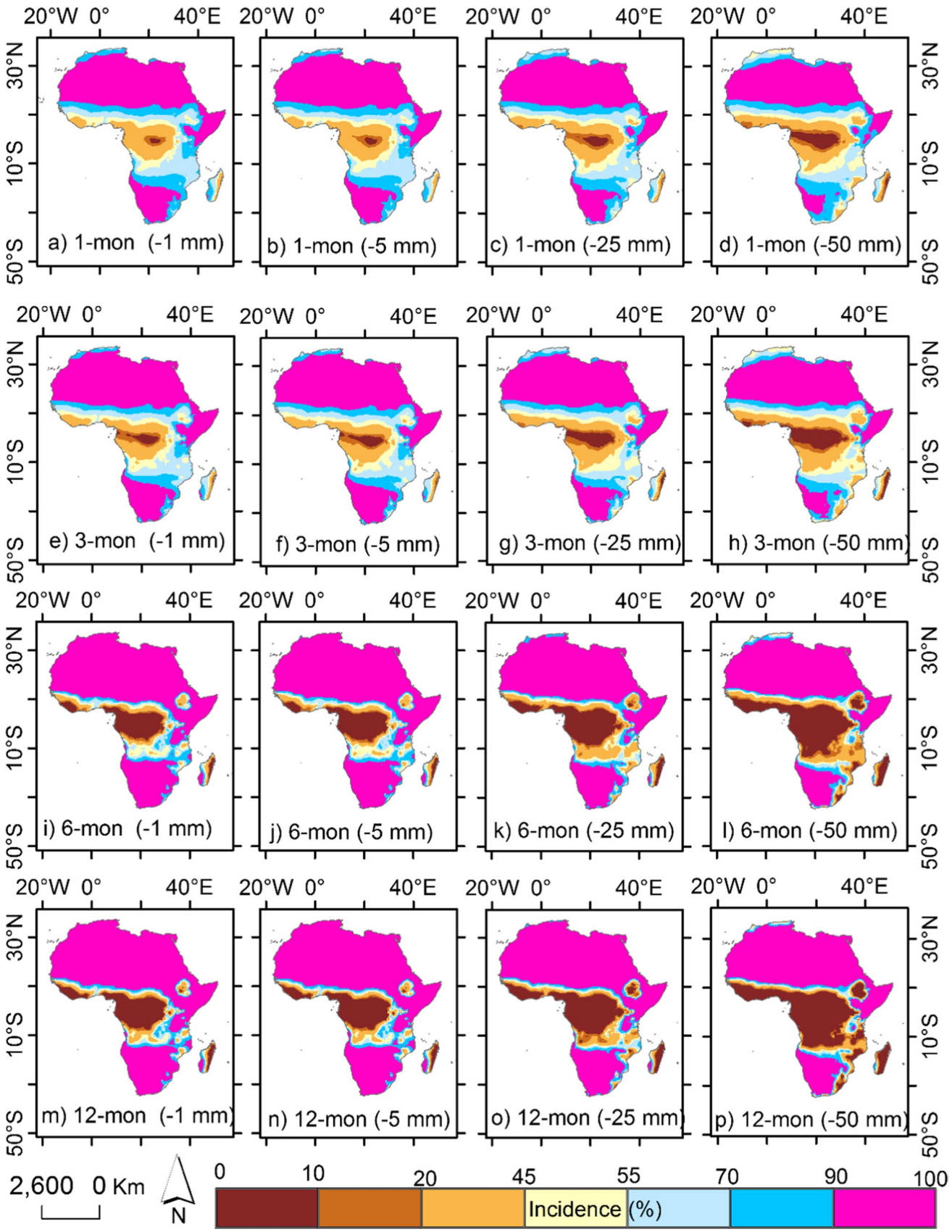

Fig. 2 Incidence of wet and dry conditions across Africa after aggregation of the CWA based on a–d 1-month, e–h 3-month, i–l 6-month, and m–p 12-month time scales. The thresholds used to obtain incidence can be seen put in "()" of the labels

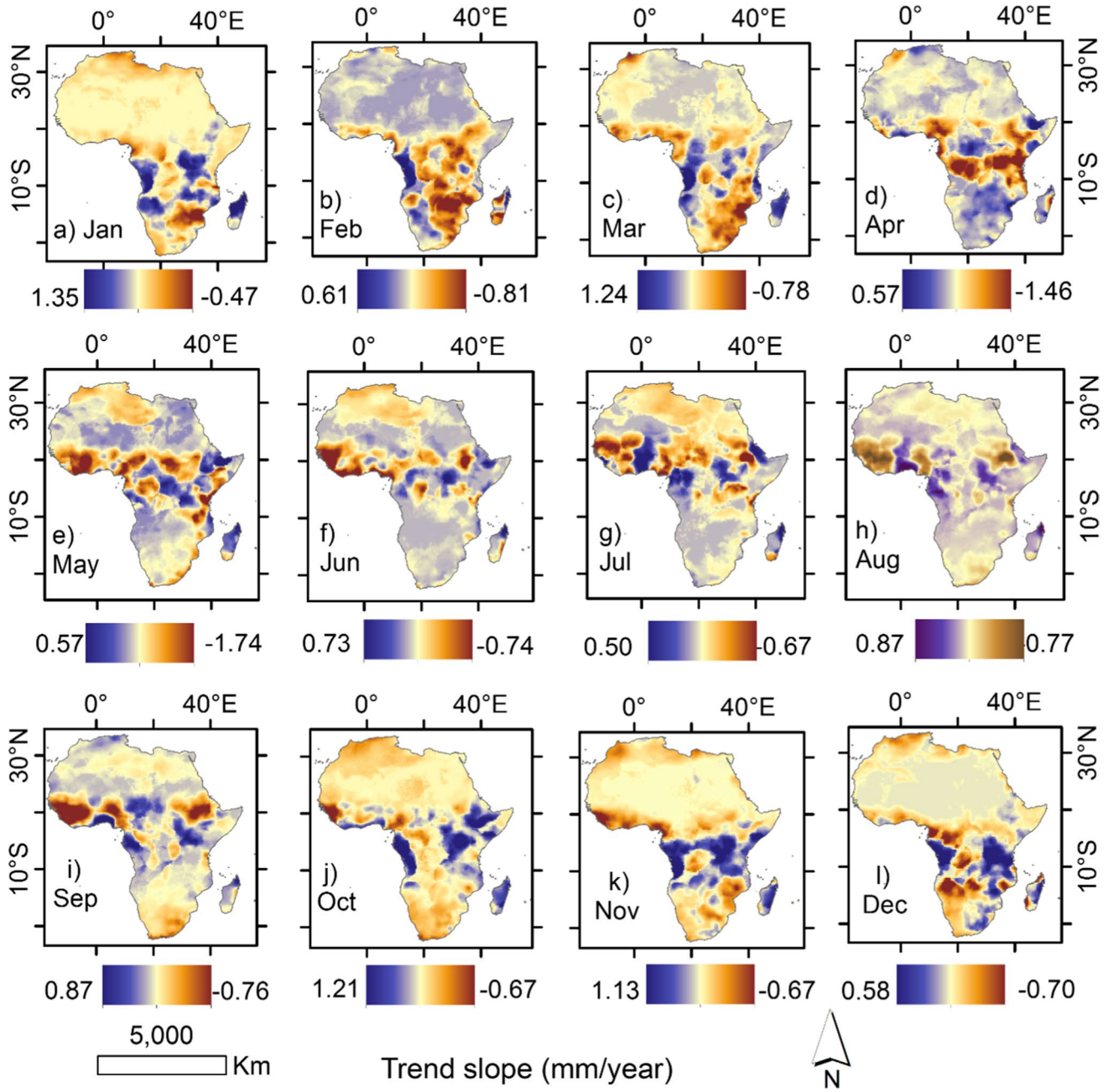

Fig. 3 Trend slope (mm/year) in 1-month aggregated CWA for a Jan, b Feb, c Mar, d Apr, e May, f Jun, g Jul, h Aug, i Sep, j Oct, k Nov, and l Dec

Furthermore, the relevance of a given time scale depends on the application for which the study is being conducted. For instance, if we are dealing with changes in terrestrial soil moisture changes with time, there is a need for monitoring transition in seasonal meteorological imbalance, and in this case, the time scale of up to 4 months can be adopted (Onyutha 2017). The time scale of 6 to 9 months can be relevant for monitoring hydrological applications (such as reservoir operations). Finally, a large time scale like 12 months can be relevant for applications which are sensitive to the alterations in groundwater levels (Onyutha 2017).

Figure 6 shows spatial distribution of drought across Africa in 1984. The Sahel region was one of the areas largely affected by extreme dry conditions. Wet conditions with SNIPE ranging from 2.00 to 2.23 (extreme wetness) were in the equatorial region in December, January, February, and March to some extent (Fig. 6a–c, l). Climatic condition of Sahara desert was also slightly wetter than the long-term mean especially in January–February-March (Fig. 6a–c) and October–November-December (Fig. 6j–l). The dry conditions with SNIPE values ranging from – 2.00

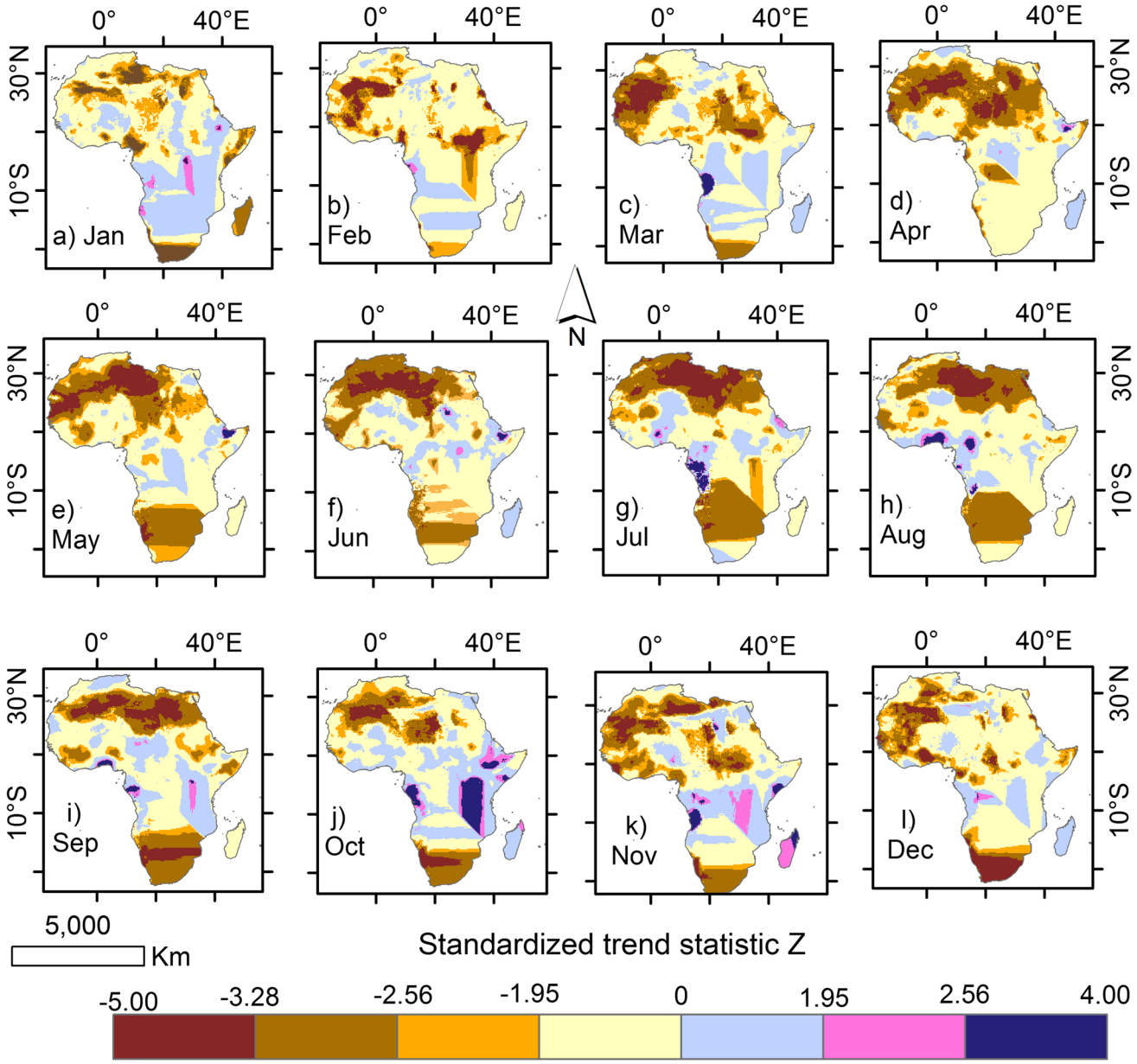

Fig. 4 Standardized trend statistic Z in 1-month aggregated CWA for a Jan, b Feb, c Mar, d Apr, e May, f Jun, g Jul, h Aug, i Sep, j Oct, k Nov, and l Dec

to − 2.23 mainly were exhibited in Ethiopia and the belt along latitude 10° N during December, January, and February (Fig. 6a–b, l). From April to August (Fig. 6d–h), the dry conditions were exhibited north of 10° N (or across the Sahara desert). In June-July–August-September, the wet conditions were mainly exhibited over West Africa especially along the coastal areas near the Gulf of Guinea (Fig. 6f–i). For September, October, and November, the dry and wet conditions were generally nearly normal (or ranging from − 0.5 to 0.5) except over Ethiopia where values of SNIPE went down to − 2.23 (extreme drought) at some locations (Fig. 6i–k).

3.4 Co-variability of SNIPE with climate indices

Figure 7 shows results of the co-variation of SNIPE along with climate indices (based on correlation analysis) across the continent. For each climate index, the magnitude of correlation coefficients varied across the vaious regions of the continent. Furthermore, the correlation across a particular region varied with time scales. For instance, SNIPE across North Africa was shown to be positively correlated with NAO (Fig. 7c, g, k, o). However, for the region between 15° N and 25° N, the correlation between SNIPE and NAO was negative (Fig. 7c, g, k, o). The SNIPE of the West

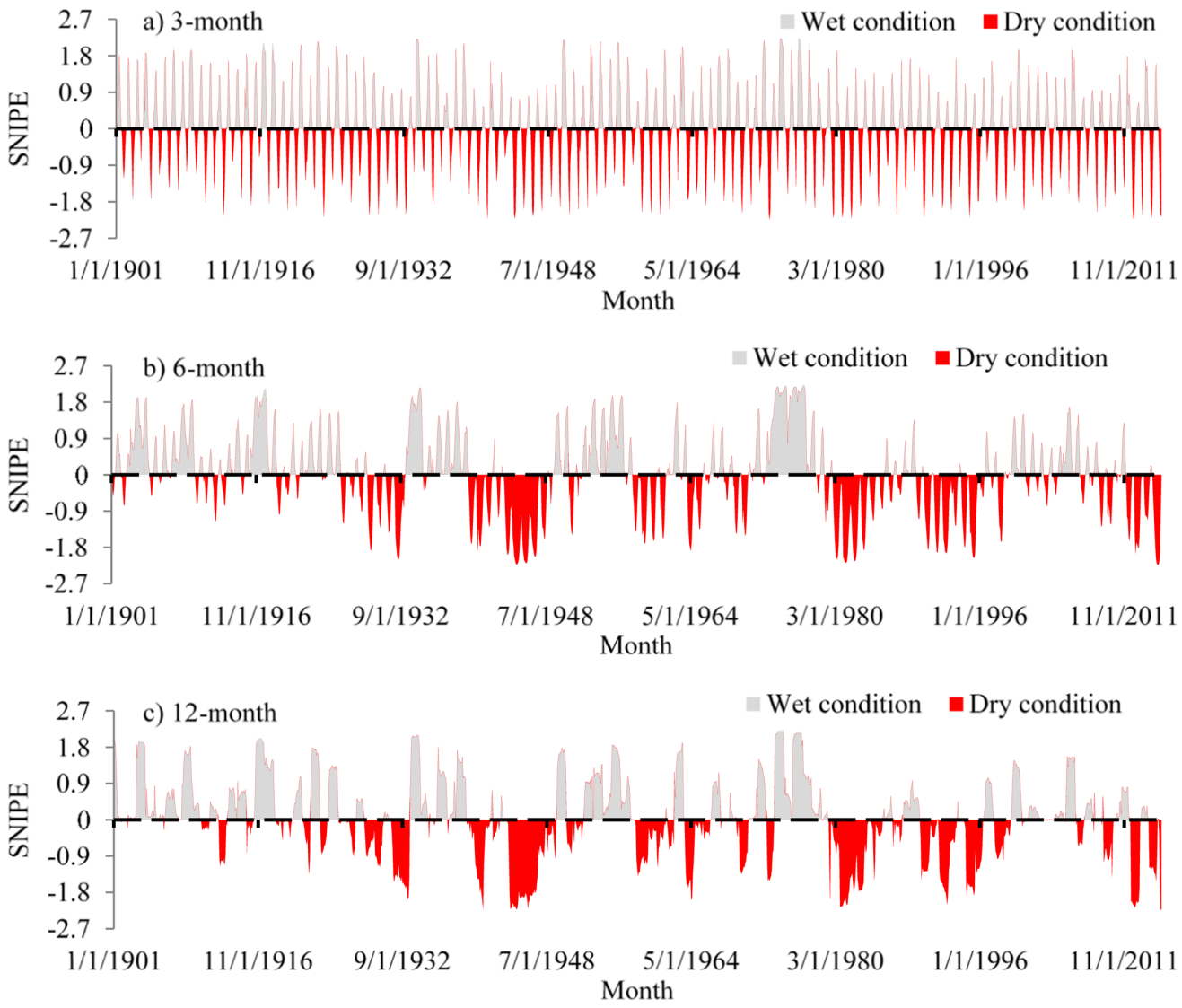

Fig. 5 The SNIPE of a 3-month, b 6-month, and c 12-month time scales for the CWA at the location with longitude = 25° and latitude = −24.75°

African region tended to be positively influenced by AMO (Fig. 7a, e, i, m). The influence of Niño 3 on the SNIPE across Sahel was mainly negative. Low rainfall across the Sahel is believed to be controlled by several factors such as ocean warming, aerosol emissions, and a southward shift of Inter Tropical Convergence Zone (Dong et al. 2014; Hwang et al. 2013; Dai 2012; Prospero and Lamb 2003; Janicot et al. 1998; Kerr 1985).

The SNIPE of all the selected time scales in the East African region was positively correlated with Niño 3 and IOD (Fig. 7b, f, j, n, d, h, l, p). This means that the variation in wet conditions across East Africa can be explained by the positive phase of theIOD and the El Niño phase of the ENSO. On the other hand, the occurrence of dry conditions across the East African region is linked to the negative phase of the IOD and cold (or La Niña) phase of the ENSO. There are several studies which found variation in the East African precipitation correlated with ENSO (Dutra et al. 2013; Le et al. 2020), or IOD (Onyutha 2018; Nicholson 2015; Liebmann et al. 2014; Tierney et al. 2013).

Contrary to the East African region, southern African droughts occur during the warm (El Niño) phase of ENSO. Precipitation in the southern part of Africa was previously found to be negatively correlated with the warm ENSO (Nicholson and Kim 1997). Another study by Rouault and Richard (2005) showed 8 out of 12 droughts detected using SPI over the southern Africa to be strongly correlated with ENSO. Other studies which found correlation between ENSO and precipitation of the southern African include Lindesay (1988), Reason et al. (2000), and Landman and Beraki (2012). However, it is vital to realize that droughts may not necessarily occur over the El Niño periods. Instead,

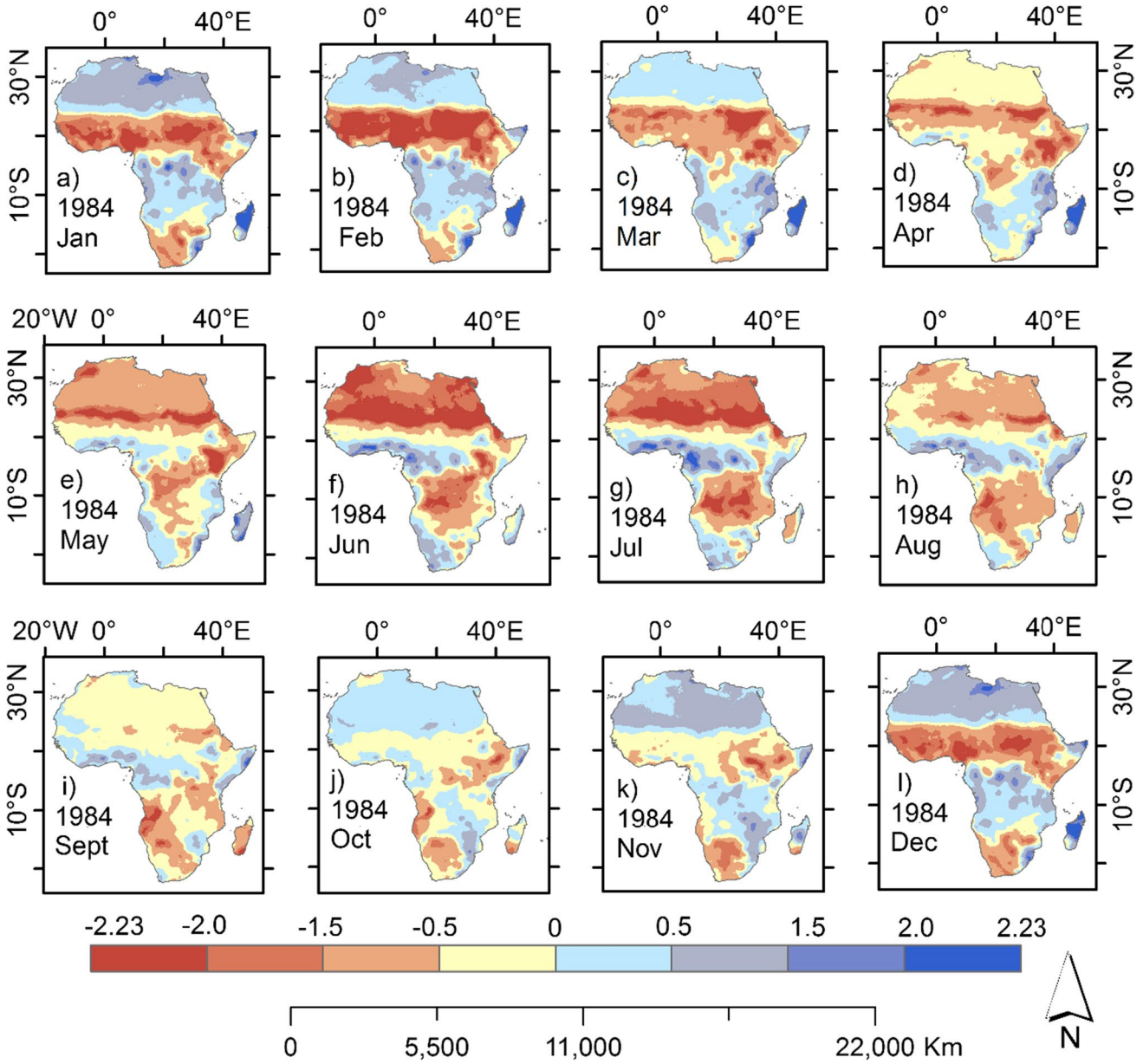

Fig. 6 Spatial distribution of 6-month SNIPE across Africa in 1984 for a Jan, b Feb, c Mar, d Apr, e May, f Jun, g Jul, h Aug, i Sep, j Oct, k Nov, and l Dec

droughts could also be caused by regional oceanic and atmospheric anomalies. For instance, March to June extreme positive Darwin sea level pressure anomalies can be additional predictor to supplement El Niño for monitoring and predicting droughts in southern Africa (Manatsa et al. 2008).

Results from Fig. 7 suggest that support of such correlation analyses for planning of predictive adaptation related to the occurrence of dry and wet conditions depends on the region being considered and the time scale selected for analyses. Furthermore, it is possible that dry or wet conditions at a particular location can synergistically be linked to two or more climate indices. In some cases, dry condition can be due to one driver while the wet season is linked to another driving force. The overall focus would on the total amount of variance that could be explained using predictors comprising combinations of various climate indices.

3.5 Predicting variation in wet and dry conditions using climate indices

Figure 8 shows the amount of variance in dry and wet conditions that could be explained by changes in large-scale ocean–atmosphere conditions. Evidently, the combined changes in temperature over the Indian Ocean (or IOD)

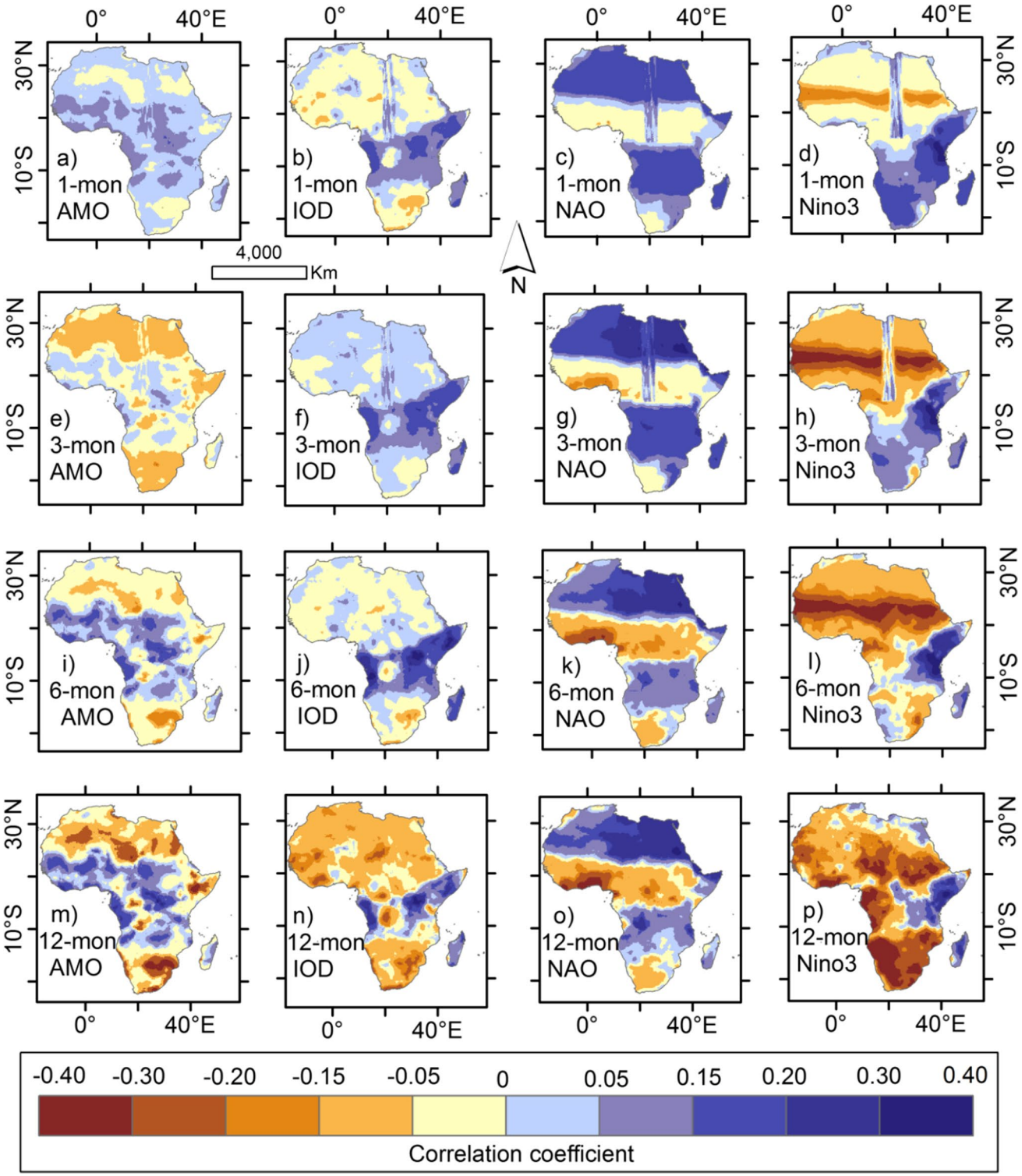

Fig. 7 Co-variation of the non-parametric indices from the difference between precipitation and PET with those obtained using AMO, IOD, NAO, and Niño 3 based on **a**–**d** 1-month, **e**–**h** 3-month, **i**–**j** 6-month, and **m**–**p** 12-month time scales

and the tropical region of the Pacific Ocean (or Niño 3) explain up to about 44% of the variance in dry and wet conditions along the Sahel belt as well as eastern part of the equatorial region (Fig. 8a). By combining IOD and NAO (Fig. 8b), IOD and AMO (Fig. 8c), and IOD, AMO, and NAO (Fig. 8f), the adjusted R^2 values remained low.

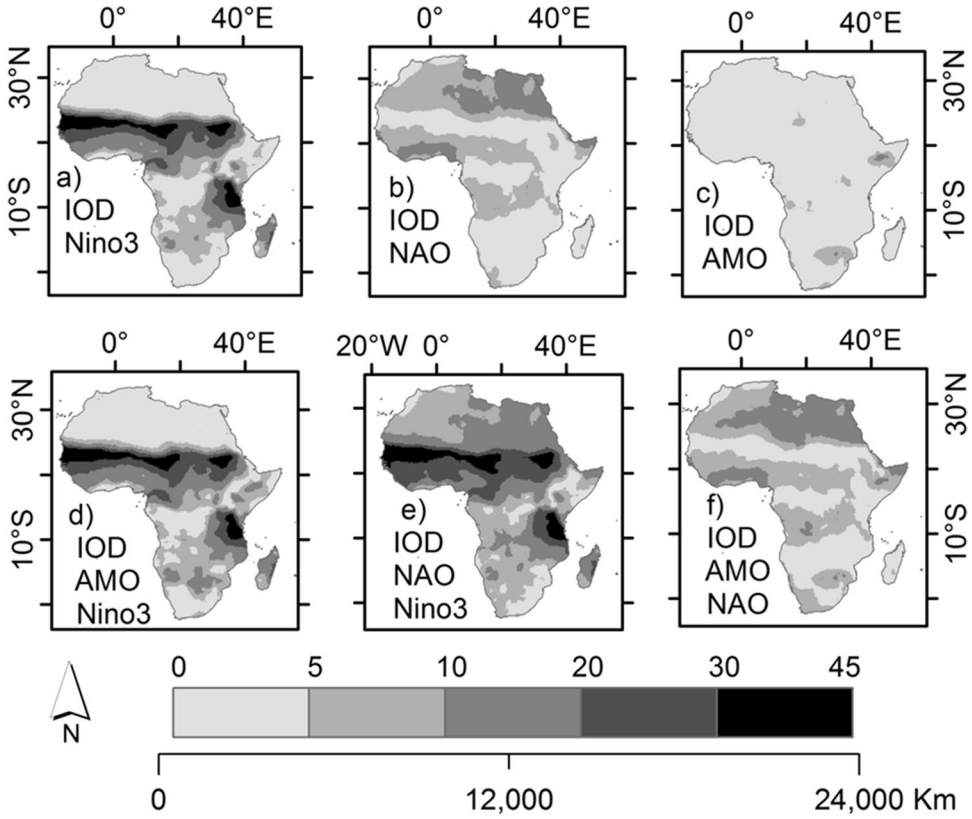

Fig. 8 Adjusted R^2 in predicting 12-month SNIPE using various **a**–**f** combinations of climate indices

For IOD and AMO (Fig. 8c), up to 15% of the variance in CWA (or SNIPE) could be explained especially in the Horn of Africa (or Somalia), and the southeastern part of Africa. Addition of either AMO (Fig. 8d) or NAO (Fig. 8e) to IOD and Niño 3 produced minimal effect on the adjusted R^2 especially across the Sahel belt and the eastern part of the equatorial region. Even when both AMO and NAO were added to IOD and Niño 3 (Fig. 9a), the result was not that very different from that in Fig. 8a.

As seen before in Fig. 7, the variation in dry and wet conditions in the Sahara desert can be mainly explained by the changes in the SLP in the North Atlantic Ocean (or NAO). In this line, combination of NAO with IOD (Fig. 8b) or AMO and IOD (Fig. 8f) had minimal effect on the adjusted R^2 across the Sahara desert. From these results, it is evident that addition of many predictors is not a guarantee to increase the values of adjusted R^2. In other words, apart from the Sahel belt and eastern part of the equatorial region which have joint influence of the ENSO and IOD, the variation in dry and wet conditions at other locations is suggestively due to one main driver.

Figure 9 shows results for predictability of the variation in dry and wet conditions using a combination of all the four climate models. Based on the results of the MLRE in terms of adjusted R^2 mapped in Fig. 9a, the amount of variance in the meteorological conditions at any selected location can be tested. To do so, the coefficients of the MLRE provided in Fig. 9b–f can be used.

The steps for predicting variation in wet and dry conditions using climate indices as predictors include the following:

i) Select the region or location to be considered; for instance, see locations numbered 1 to 8 in Fig. 10.
ii) For each selected location, determine the coefficients of the MLRE from Fig. 9b–f. For illustration considering the 8 locations shown in Fig. 10, the coefficients of the MLRE obtained from Fig. 9b–f can be seen in Table 2.
iii) For a selected location, the identified coefficients of the MLRE can be fed into Eq. (12) using selected combination of climate indices to obtain an adjusted R^2. Results of this step based on the 8 selected locations can be seen in Table 3.

It is noticeable from Table 3 that the amount of variance in the CWA that can be explained by climate indices varies among locations. However, the main contribution to the overall amount of variance explained comes from the dominant driver. For instance, at locations 1 and 5, the main driving forces are in the form of Niño 3 and IOD, respectively. This means that in the build-up of MLRE to predict dry and wet conditions for a particular region, selection of the main

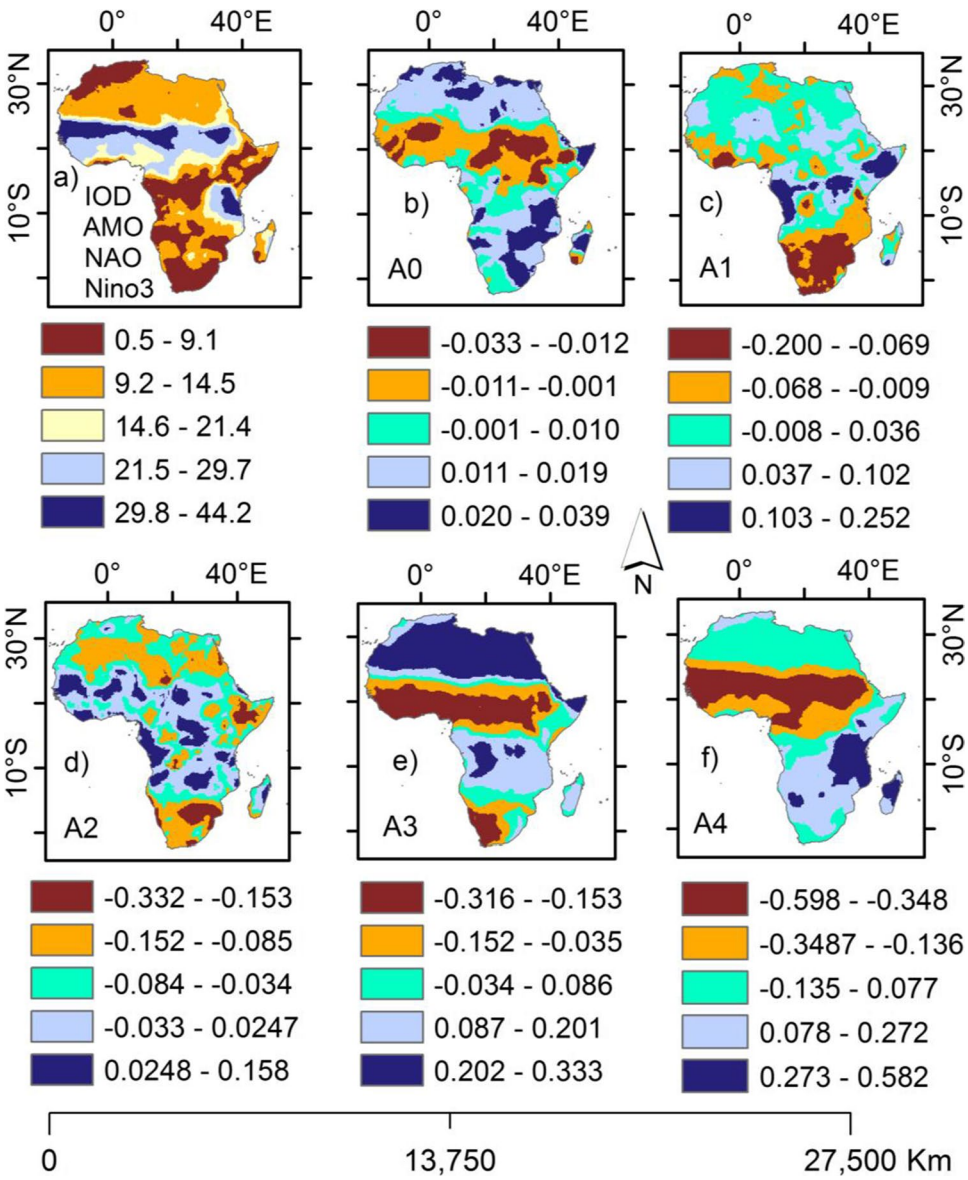

Fig. 9 Adjusted R^2 in predicting 12-month SNIPE using a combination of four climate indices based on **b**–**f** various coefficients of the MLRE

driver comprises a crucial step. If drivers of the variation in dry and wet conditions are known, there can be improvement in the forecasting and warning systems for predictive planning of water resources applications in the affected region.

4 Conclusions

This study characterized wet and dry conditions across the African continent using standardized non-parametric indices of precipitation and PET (SNIPE). The difference between precipitation and potential evapotranspiration (PET) (taken to be CWA) was computed from monthly datasets of the Climatic Research Unit (RCU). These CRU time series were in a gridded ($0.5° \times 0.5°$) form covering the period 1901–2015. This study assessed trends, variability, and drought incidence based on CWA. Multiple linear regression (MLR) was used to test the predictability of the variation in wet and dry conditions while taking into account possible difference in the regional hydroclimate.

Low drought incidents or large positive values of the CWA (ranging from moderate to extreme wetness) were confined to areas that receive large amounts of precipitation. Areas with low drought incidence included the region along the Gulf of Guinea, the western part of the equatorial region, and the Ethiopian Highlands. The Tropics were characterized by positive trends in the CWA (or wetting trends). However, most of these wetting trends were mostly insignificant ($p > 0.05$). Areas outside the Tropics were mainly characterized by negative trends in CWA (or drying trends). These drying trends which largely occurred in the CWA of

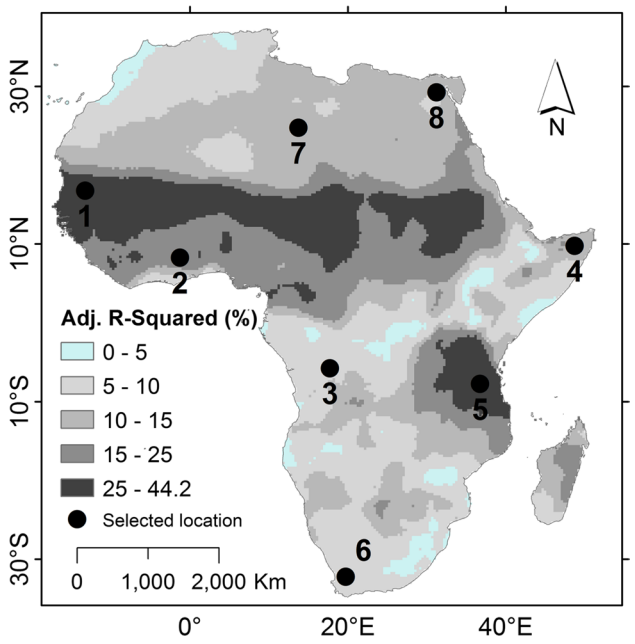

Fig. 10 Location at which the 12-month SNIPE was predicted using a combination of the four selected climate indices

April, May, June, July, August, and September were mainly significant ($p < 0.05$) over the Sahara desert.

Variation in the East African CWA was positively correlated with Niño 3 and IOD. CWA variability in the southern Africa was negatively correlated with Niño 3. Variability of CWA across West Africa (or Sahel) was negatively correlated with Niño 3 and also linked to changes in the sea surface temperature over the Atlantic Ocean. The strength of the co-variability of dry and wet conditions across any region depended on the time scale used for analysis.

Results of predictability of variation in wet and dry conditions using combinations of climate indices varied across regions and among time scales. For instance, using combination of IOD and Niño 3 as predictors, less than 10% of the total variance in CWA of 12-month time scale across the Sahara desert could be explained. However, up to about 40% of the total variance in 12-month CWA across East Africa could be explained using IOD and Niño 3 as predictors.

An important remark is that due to some factors such as the high signal-to-noise ratio and inter-correlation among the climate indices, the correlation between SNIPE and climate indices may not be indicative of the actual dynamics of how

Table 2 Coefficients of the MLRE when all the four climate indices were combined as a predictor

Location	1	2	3	4	5	6	7	8
A0	0.001	−0.003	0.013	0.022	0.027	0.003	0.019	0.021
A1	0.009	−0.022	0.008	0.081	−0.031	−0.087	0.001	0.034
A2	0.054	−0.046	0.027	−0.100	0.034	−0.117	−0.087	−0.010
A3	−0.056	−0.305	0.270	0.251	0.168	−0.212	0.281	0.279
A4	−0.591	−0.276	0.042	0.110	0.573	0.031	−0.031	0.012

Table 3 Adjusted R^2 (%) in predicting 9-month SNIPE using climate indices

Location	1	2	3	4	5	6	7	8
AMO (A)	0.187	0.009	0.001	1.412	0.010	1.100	1.679	0.213
NAO (N)	0.178	*8.505*	*1.986*	*2.398*	1.714	*4.381*	*4.168*	*3.875*
IOD (I)	1.638	0.431	0.066	0.335	*12.806*	0.683	0.557	0.023
Niño 3 (E)	*17.109*	1.410	0.494	0.074	08.158	0.494	1.985	0.806
I, A	2.153	0.535	0.005	2.673	0.956	1.826	1.967	0.250
I, N	2.836	**12.937**	8.964	9.594	6.011	5.574	10.567	**9.799**
I, E	**43.622**	10.824	0.432	2.562	**40.529**	0.864	0.247	0.139
A, N	1.296	12.263	9.008	9.424	4.869	**6.413**	**11.440**	9.650
A, E	44.048	10.834	0.415	4.146	40.326	1.291	1.927	0.353
N, E	44.071	21.637	**9.145**	**10.526**	43.725	4.394	10.651	9.695
I, A, E	44.068	10.835	0.436	4.573	40.550	1.858	1.981	0.367
I, N, E	44.105	21.739	9.164	11.033	43.801	5.698	10.669	9.816
A, N, E	44.445	21.932	9.243	11.446	43.826	6.429	11.554	9.698
I, A, N	3.283	13.152	9.048	10.795	6.094	7.188	11.444	9.811
I, A, N, E	44.453	21.989	9.251	12.201	43.933	7.301	11.554	9.828

Italicized values are the adjusted R^2 for the best climate index used as a predictor while values in bold are the adjusted R^2 for the best predictor comprising two climate indices

changes in SST or SLP from various oceans affect the dry and wet conditions across Africa. In other words, the correlation between SNIPE and climate indices may be taken to merely indicate statistical measures of association. Furthermore, for brevity, the lag or precedence of the SNIPE by climate indices was not considered. It is also worth noting that relationship between CWA and climate indices may be linear or non-linear. Although linear model was selected in this study, it is recommended that future research considers the suitability of linear and non-linear models to test the predictability of the variation in dry and wet conditions across the various regions of Africa. Furthermore, predictability of the variation in wet and dry conditions across the continent was tested using a single time scale. It is recommended that future research takes into account possible differences in predictability of variations in wet and dry conditions due to the influence from the choice of time scales. Nevertheless, results from this study can importantly be used to support planning or strategies for management of risks related to extreme dry and wet conditions across the continent of Africa.

Acknowledgements The author acknowledges that the data used in this study were from the Climatic Research Unit (CRU) (i.e., Time-Series (TS) version 4.0 or CRU TS4.0).

Author contribution The entire work under this study was solely undertaken by the sole author.

Availability of data and material The link that can be used to download the data used in this study was provided within the paper.

Code availability The codes used for computing SNIPE and detecting trends can be obtained from the author upon request.

Declarations

Ethics approval This research did not involve human subjects. Meteorological datasets used in this study can all be obtained from publicly accessible archives.

Consent to participate This research did not involve human subjects.

Consent for publication This research did not involve personal information for which consent was to be sought.

Conflict of interest The author declares no competing interests.

References

Almazroui M, Saeed F, Saeed S, Islam MN, Ismail M, Klutse NAB, Siddiqui MH (2020) Projected change in temperature and precipitation over Africa from CMIP6. Earth Syst Environ 4:455–475

Dai AG (2012) Drought under global warming: a review. Wiley Interdiscip Rev-Clim Change 3(6):617

Delworth TL, Mann ME (2000) Observed and simulated multi-decadal variability in the Northern Hemisphere. Clim Dyn 16:661–676

Dong B, Sutton RT, Highwood E, Wilcox L (2014) The impacts of European and Asian anthropogenic sulfur dioxide emissions on Sahel precipitation. J Clim 27:7000–7017

Dutra E, Magnusson L, Wetterhall F, Cloke HL, Balsamo G, Boussetta S, Pappenberger F (2013) The 2010–2011 drought in the Horn of Africa in ECMWF reanalysis and seasonal forecast products. Int J Climatol 33:1720–1729

Ezekiel M (1930) Methods of correlational analysis. New York: Wiley

Folland CK, Parker DE, Palmer TN (1986) Sahel rainfall and worldwide sea temperatures, 1901–85. Nature 320:602–607

Gebremeskel G, Tang Q, Sun S, Huang Z, Zhang X, Liu X (2019) Droughts in East Africa: causes, impacts and resilience. Earth-Sci Rev 193:146–161

Harris I, Jones PD, Osborn TJ, Lister DH (2014) Updated high resolution grids of monthly climatic observations–the CRU TS3.10 dataset. Int J Climatol 34:623–642

Hillbruner C, Moloney G (2012) When early warning is not enough—lessons learned from the 2011 Somalia Famine. Glob Food Sec 1:20–28

Horel JD (1982) On the annual cycle of the tropical Pacific atmosphere and ocean. Mon Weather Rev 110:1863–1878

Hwang Y-T, Frierson DMW, Kang SM (2013) Anthropogenic sulfate aerosol and the southward shift of tropical precipitation in the late 20th century. Geophys Res Lett 40:1–6

Ilori OW, Ajayi VO (2020) Change detection and trend analysis of future temperature and rainfall over West Africa. Earth Syst Environ 4:493–512

Janicot S, Harzallah A, Fontaine B, Moron V (1998) West African monsoon dynamics and Eastern Equatorial Atlantic and Pacific SST anomalies (1970–88). J Clim 11:1874–1882

Jones PD, Jonsson T, Wheeler D (1997) Extension to the North Atlantic oscillation using early instrumental pressure observations from Gibraltar and south-west Iceland. Int J Climatol 17(13):1433–1450

Kerr RA (1985) Fifteen years of African drought. Science 227(4693):1453–1454

Klutse NAB, Quagraine KA, Nkrumah F, Quagraine KT, Berkoh-Oforiwaa B, Dzrobi JF, Sylla MB (2021) The climatic analysis of summer monsoon extreme precipitation events over West Africa in CMIP6 simulations. Earth Syst Environ 5:25–41

Knudsen M, Jacobsen B, Seidenkrantz MS et al (2014) Evidence for external forcing of the Atlantic Multidecadal Oscillation since termination of the Little Ice Age. Nat Comm 5:3323. https://doi.org/10.1038/ncomms4323

Landman WA, Beraki A (2012) Multi-model forecast skill for midsummer rainfall over southern Africa. Int J Climatol 32(2):303–314

Le JA, El-Askary HM, Allali M, Sweliem H, Piechota TC, Struppa DC (2020) Characterizing El Niño-Southern Oscillation effects on the Blue Nile Yield and the Nile River Basin precipitation using empirical mode decomposition. Earth Syst Environ 4:699–711

Liebmann B, Hoerling MP, Funk C, Bladé I, Dole RM, Allured D, Quan X, Pegion P, Eischeid JK (2014) Understanding recent Eastern Horn of Africa rainfall variability and change. J Clim 27 (23):8630–8645

Lindesay JA (1988) South African rainfall, the southern oscillation and a southern hemisphere semi-annual cycle. J Climatol 8(1):17–30

Lyon B (2014) Seasonal drought in the Greater Horn of Africa and its recent increase during the March-May long rains. J Clim 27(21):7953–7975

Manatsa D, Chingombe W, Matsikwa H, Matarira CH (2008) The superior influence of Darwin sea level pressure anomalies over ENSO as a simple drought predictor for Southern Africa. Theor Appl Climatol 92:1–14

Mann ME, Zhang Z, Rutherford S, Bradley RS, Hughes MK, Shindell D et al (2009) Global signatures and dynamical origins of the little ice age and medieval climate anomaly. Science 326:1256–1260

McKee T, Doesken N, Kleist J (1993) The relationship of drought frequency and duration to time scales. In: Proceedings of the 8th Conference of Applied Climatology. Anaheim: American Meteorological Society, pp. 179–184

Mwangi E, Wetterhall F, Dutra E, Di Giuseppe F, Pappenberger F (2014) Forecasting droughts in East Africa. Hydrol Earth Syst Sci 18(2):611–620

Nicholson SE (2014) A detailed look at the recent drought situation in the Greater Horn of Africa. J Arid Environ 103:71–79

Nicholson SE (2015) Long-term variability of the East African 'short rains' and its links to large-scale factors. Int J Climatol 35(13):3979–3990

Nicholson SE, Kim J (1997) The relationship of the El Niño–southern oscillation to African rainfall. Int J Climatol 17:117–135

Ntale HK, Gan TY (2003) Drought indices and their application to East Africa. Int J Climatol 23(11):1335–1357

Omute P, Corner R, Awange JL (2012) The use of NDVI and its derivatives for monitoring Lake Victoria's water level and drought conditions. Water Resour Manage 26(6):1591–1613

Onyutha C (2017) On rigorous drought assessment using daily time scale: non-stationary frequency analyses, revisited concepts, and a new method to yield non-parametric indices. Hydrology 4(4):48. https://doi.org/10.3390/hydrology4040048

Onyutha C (2018) Trends and variability in African long-term precipitation. Stoch Environ Res Risk Assess 32:2721–2739. https://doi.org/10.1007/s00477-018-1587-0

Onyutha C (2019) Hydrological model supported by a step-wise calibration against sub-flows and validation of extreme flow events. Water 11(2):244. https://doi.org/10.3390/w11020244

Onyutha C (2020a) Analyses of rainfall extremes in East Africa based on observations from rain gauges and climate change simulations by CORDEX RCMs. Clim Dyn 54:4841–4864

Onyutha C (2020b) Trends and variability of temperature and evaporation over the African continent: relationships with precipitation. Atmósfera. https://doi.org/10.20937/ATM.52788

Onyutha C (2021) Graphical-statistical method to explore variability of hydrological time series. Hydrol Res 52(1):266–283

Onyutha C, Willems P (2017) Space-time variability of extreme rainfall in the River Nile basin. Int J Climatol 37(4):4915–4924

Otterå OH, Bentsen M, Drange H, Suo L (2010) External forcing as a metronome for Atlantic multidecadal variability. Nat Geosci 3:688–694

Parker D, Folland C, Scaife A, Knight J, Colman A, Baines P, Dong B (2007) Decadal to multidecadal variability and the climate change background. J Geophys Res 112:D18115. https://doi.org/10.1029/2007JD008411

Prospero JM, Lamb PJ (2003) African droughts and dust transport to the Caribbean: climate change implications. Science 302(5647):1024–1027. https://doi.org/10.1126/science.1089915

Rayner NA, Parker DE, Horton EB, Folland CK, Alexander LV, Rowell DP, Kent EC, Kaplan A (2003) Global analyses of sea surface temperature, sea ice, and night marine air temperature since the late nineteenth century. J Geophys Res 108(D14):4407

Reason CJC, Allan RJ, Lindesay JA, Ansell TJ (2000) ENSO and climatic signals across the Indian Ocean Basin in the global context. Part I: Interannual composite patterns. Int J Climatol 20(11):1285–1327

Rojas O, Vrieling A, Rembold F (2011) Assessing drought probability for agricultural areas in Africa with coarse resolution remote sensing imagery. Remote Sens Environ 115:343–352

Rouault M, Richard Y (2005) Intensity and spatial extent of droughts in southern Africa. Geophys Res Lett 32:L15702. https://doi.org/10.1029/2005GL022436

Sen PK (1968) Estimates of the regression coefficient based on Kendall's tau. J Am Stat Assoc 63:1379–1389

Shanko D, Camberlin P (1998) The effects of the Southwest Indian Ocean tropical cyclones on Ethiopian drought. Int J Climatol 18(12):1373–1388

Sheffield J, Wood EF, Chaney N, Guan K, Sadri S, Yuan X, Olang L, Amani A, Ali A, Demuth S, Ogallo L (2014) A drought monitoring and forecasting system for sub-Sahara African water resources and food security. Bull Am Meteorol Soc 95(6):861–882

Shiferaw B, Tesfaye K, Kassie M, Abate T, Prasanna BM, Menkir A (2014) Managing vulnerability to drought and enhancing livelihood resilience in sub-Saharan Africa: technological, institutional and policy options. Weather Clim Extr 3:67–79

Theil H (1950) A rank-invariant method of linear and polynomial regression analysis. Neder Akad Wet Ser A 53:386–392

Tierney JE, Smerdon JE, Anchukaitis KJ, Seager R (2013) Multidecadal variability in East African hydroclimate controlled by the Indian Ocean. Nature 493:389–392

Trenberth K (1997) The definition of El Niño? Bull Am Meteorol Soc 78(12):2771–2777

Uhe P, Philip S, Kew S, Shah K, Kimutai J, Mwangi E, van Oldenborgh GJ, Singh R, Arrighi J, Jjemba E, Cullen H (2017) Attributing drivers of the 2016 Kenyan drought. Int J Climatol 38:554–568

van Oldenborgh GJ, te Raa LA, Dijkstra HA, Philip SY (2009) Frequency- or amplitude-dependent effects of the Atlantic meridional overturning on the tropical Pacific Ocean. Ocean Sci 5:293–301

Verschuren D, Laird KR, Cumming BF (2000) Rainfall and drought in equatorial east Africa during the past 1,100 years. Nature 403(6768):410–414

Vicente-Serrano SM, Beguería S, López-Moreno JI (2010) A multiscalar drought index sensitive to global warming: the standardized precipitation evapotranspiration index. J Clim 23:1696–1718

Viste E, Korecha D, Sorteberg A (2013) Recent drought and precipitation tendencies in Ethiopia. Theor Appl Climatol 112(3–4):535–551

Zhao T, Dai A (2015) The magnitude and causes of global drought changes in the twenty-first century under a low–moderate emissions scenario. J Clim 28(11):4490–4512